Heliyon 10 (2024) e30349

Contents lists available at ScienceDirect

Heliyon

journal homepage: www.cell.com/heliyon

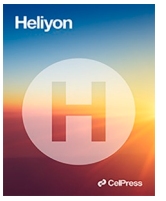

Research article

# Functionalization of β-cyclodextrin metal-organic frameworks with gelatin and glutamine for drug delivery of curcumin to cancerous cells

Pegah Sadeh [a], Sedigheh Zeinali [a,*], Banafsheh Rastegari [b], Iman Najafipour [a]

[a] Department of Nanochemical Engineering, School of Advanced Technologies, Shiraz University, Iran
[b] Diagnostic Laboratory Sciences and Technology Research Center, School of Paramedical Sciences, Shiraz University of Medical Science, Shiraz, Iran

ARTICLE INFO

*Keywords:*
Drug delivery
Metal-organic framework
Amine-functionality
Cyclodextrin
Glutamine

ABSTRACT

Beta-cyclodextrin Metal-Organic Framework (β-CD-MOF) is a unique class of porous materials that merges the inherent properties of cyclodextrins with the structural advantages of metal-organic frameworks (MOFs). When combined with the concept of MOFs, which are crystalline structures composed of metal ions or clusters linked by organic ligands, the resulting β-CD-MOF holds immense potential for various applications, especially in the field of drug delivery. In this study, biocompatible metal-organic frameworks (MOFs) synthesized using β-Cyclodextrin (β-CD) and potassium enabled drug delivery of curcumin (CCM) to cancerous cells. Functionalizing β-CD-MOF with L-glutamine (glutamine-β-CD-MOF) enhanced cancer cell-specific targeting due to glutamine's essential role in cancer cell proliferation and energy pathways. Amino group functionalization provided further functionalization opportunities. Gelatin coating (gelatin@β-CD-MOF) facilitated controlled drug release in an acidic medium. High drug loading capacities (52.38–55.63 %) were achieved for β-CD-MOF@CCM and glutamine-β-CD-MOF@CCM, leveraging the high porosity and affinity of amine and phenol groups of curcumin. The MTT assay highlighted the specificity and differentiation of glutamine-β-CD-MOF in targeting cancerous over normal cells. These functionalized β-CD MOFs efficiently encapsulate curcumin, ensuring controlled drug release and enhanced therapeutic efficacy, particularly in cancer therapy.

## 1. Introduction

Cancer is one of the leading causes of global mortality. Conventional treatments, including radiotherapy, surgery, immunotherapy, and chemotherapy, are yet to achieve complete therapeutic success [1]. Nanotechnology is extensively utilized for therapeutic and diagnostic development. Their properties have made them lucrative candidates for drug delivery systems [2]. Metal-organic frameworks (MOFs) are a class of microporous crystalline coordination polymers consisting of metal nodes or clusters interconnected with these materials [3–6]. The exceptional porosity and high surface area of these structures, together with tuning and designing of a variety of MOFs due to infinite combination of metal nodes and organic ligands, tailorable pore size, biocompatibility and biodegradability, and ease of functionalization of organic ligands, led to the vast potential and application of ions utilized in the synthesis include p-block elements, transition metals, alkaline earth metals, alkaline metals, lanthanides, and actinides [7]. Diverse applications

* Corresponding author.
*E-mail addresses:* zeinali@shirazu.ac.ir, zzeinali@yahoo.com (S. Zeinali).

https://doi.org/10.1016/j.heliyon.2024.e30349
Received 29 July 2023; Received in revised form 23 April 2024; Accepted 24 April 2024
Available online 25 April 2024

of MOFs including gas storage, adsorption, separation, ion exchange, molecular recognition, sensing and detection, optics, catalysis, electrocatalysis, photovoltaics, imaging, and drug delivery are introduced [8–17]. MOFs have been considered promising carriers in drug delivery systems, due to their high storage capacity and controlled release. Their crystalline nature combined with high porosity enables high drug loading [18]. However, the intrinsic toxicity and low biocompatibility of many organic ligands and metal nodes hinder their biological applications [19].

In this regard, biological metal-organic frameworks (BioMOFs) have been developed, which are a new class of MOFs with biological ligands, including nucleobases, amino acids, peptides, and saccharides that offer a higher degree of biocompatibility, biodegradability, and reduced level of cytotoxicity [19,20]. Carbohydrates, including oligosaccharides and polysaccharides, are recognized edible materials. The biocompatibility and biodegradability of carbohydrates make them unique candidates for drug delivery [21]. Cyclodextrins (CDs) are a class of carbohydrates derived from glucose polymers, that are composed of cyclic oligosaccharides with various d-glucopyranose units linked with α-1,4 glycosidic bonds. Beta cyclodextrin (β-CD) is often chosen due to its versatile cavity size, suitable for encapsulating a wide range of guest molecules. It offers better aqueous solubility, stability, and high complexation efficiency, making it a preferred choice for drug delivery, food, and various applications. Additionally, its widespread commercial availability and proven biocompatibility contribute to its popularity over alpha and gamma cyclodextrins. The conical structures of CDs consist of an outer hydrophilic surface formed with hydroxyl groups, while the inner hydrophobic surface is formed from C–H units and glycosidic linkage [22]. These CDs can be merged into MOFs creating CD-MOFs with alkali metals as nodes, hence, eliminating the need for heavy metals which are a potential source for cytotoxicity [21,23]. β-CD-MOFs, owing to their unique properties such as high porosity, tunable structures, and biocompatibility, have demonstrated exceptional potential in delivering therapeutic agents to specific cellular targets. The design and application of β-CD MOFs in drug delivery have garnered significant attention due to their ability to encapsulate a diverse range of drugs, including hydrophobic and hydrophilic compounds. These versatile carriers offer a controlled and sustained release of drugs, crucial for enhancing therapeutic efficacy while minimizing adverse effects. Moreover, their surface functionalization allows for further tailoring, enabling targeted delivery to specific cells or tissues [22].

Curcumin is a major bioactive component of turmeric [24]. Curcumin is an effective anti-inflammatory, anti-diabetic, anti-oxidant, anti-arthritic agent, and anti-proliferative natural product. It also has the anti-carcinogenic and anti-metastatic effect, which involves apoptotic potential against different cancerous cells, influences major cell signaling pathways, and angiogenesis inhibition, respectively [25]. Notably, curcumin has a significantly higher $IC_{50}$ in healthy cells than in cancerous ones which are so-called "selective anticancer" agents [26]. Curcumin, a hydrophobic polyphenolic compound, has poor solubility in the aqueous medium and low bioavailability [27]. Therefore, a nanocarrier is introduced for the loading and delivery of curcumin to increase cellular uptake. Curcumin has been previously encapsulated in different materials, including gelatin, liposomes, cationic micelles, modified starch, and CDs. Curcumin can be encapsulated in the hydrophobic cavity of Cyclodextrins in which one of the two phenyl rings of curcumin is encapsulated [28]. CDs are beneficial in pharmaceutics due to the formation of inclusion complexes with drug molecules. Upon the formation of inclusion complexes significant changes, including enhanced solubility, physical and chemical stability, and other physicochemical properties in drugs occur. These enhancements result in improved biological performance [29]. Moreover, to increase the efficiency of drug delivery and drug release, the structures can be coated with biopolymers and targeting moieties.

Gelatin, a natural biopolymer, is safe to use in a wide range of medical applications. Gelatin can help modulate the release of therapeutic agents over prolonged durations. Controlled release of nanocarriers can be necessary to reduce the intake and dosage of the administered drug in patients [30,31]. Glutamine, an abundant amino acid in our body, is a nutrient that participates in energy formation, signaling, and macromolecular synthesis in cancer cells. Thus, glutamine can be utilized as a bait molecule for targeted drug delivery applications [32]. This research aims to functionalize β-CD-MOFs with L-glutamine and coat it with gelatin for the delivery of the hydrophobic drug, curcumin, for targeting cancerous cells. L-glutamine will be used for the first time as the targeting moiety for cancer cells as this research aims to exploit tumor cell glutamine dependence. Furthermore, the β-CD MOFs were coated with gelatin for the first time for modulating drug release in the acidic and normal environment. To the author's best knowledge, no previous investigation has been conducted on the functionalization of β-CD-MOF for increasing the controlled release efficiency and for targeting using an amino acid.

## 2. Materials and methods

### 2.1. Materials and chemicals

The β-CD-MOF was obtained from ACROS Chemicals. Potassium hydroxide (KOH), cetyltrimethylammonium bromide (CTAB), ethanol (EtOH), methanol (MeOH), isopropanol ($^{i}$PrOH), sodium periodate ($NaIO_4$), gelatin, and glutaraldehyde were purchased from Merck (Darmstadt, Germany). L-glutamine and bovine serum albumin (BSA) were purchased from Sigma Aldrich (St. Louis, MO, USA). The curcumin was gifted from Karen critical pharmaceutical and nutritional supplements company, in Tehran, Iran.

### 2.2. The synthesis procedure of β-CD-MOF

The vapor diffusion method was used for the synthesis of β-CD-MOF. 1 mmol of KOH (56 mg) and 0.125 mmol of β-CD (141.8 mg) were placed in 5 ml of distilled water and stirred at 500 rpm for 30 min. The colorless solution was passed through a 0.22-μm syringe filter and added to 0.5 ml of methanol in a glass tube. Subsequently, methanol was allowed to vapor diffuse into the solution at 60 °C for 24 h. This solution was added to a solution containing 112 mg of CTAB dissolved in 7 ml of MeOH and left overnight. Then the final solution was centrifuged at 5000 rpm for 10 min. The precipitates were separated and washed three times with isopropanol, and were

dried in an oven for 24 h at 50 °C [33].

### 2.3. Characterization methods of β-CD-MOF

#### 2.3.1. XRD

The crystalline diffraction pattern analysis of particles was performed using X-ray diffraction (XRD) D8 Advanced, Bruker, Germany equipped with Cu- Kα radiation (λ = 1.54060 Å) source. The measurements were performed from 5° to 50°. The tube voltage, current, and scan speed were 40 kV, 40 mA, and 0.05°/min, respectively.

#### 2.3.2. FTIR

The functional groups were studied using a Fourier transform infrared spectrometer (FTIR) Tensor II of Bruker (Bruker Biospin, Rheinstetten, Germany). The wavenumber was set within the range of 4000 $cm^{-1}$ to 400 $cm^{-1}$ with a resolution of 4 $cm^{-1}$.

#### 2.3.3. NMR

All $^{1}$HNMR measurements were performed on a Bruker Avance 400 MHz Ultrashield spectrometer (Bruker Biospin, Rheinstetten, Germany). The chemical shifts are presented in terms of parts per million (ppm).

#### 2.3.4. SEM

Scanning electron microscopy imaging VEGA TS 5136 LSU (Tescan, Czech Republic) was used to observe particle morphology, and size at 40 kV. The particles were coated with gold using a gold sputter DSR. ImageJ software was utilized for the investigation of the sizes of particles.

#### 2.3.5. UV–Vis

The absorbance of curcumin in drug loading and release was measured in a UV–Vis spectrophotometer (UNICO Spectrophotometer Model UV2150, Santa Clara, CA, USA) with a quartz cell.

### 2.4. Functionalization of β-CD-MOF with L-glutamine

#### 2.4.1. Aldehyde- β-CD-MOF

40 mg of $NaIO_4$ was dissolved in 2 ml of distilled water and was added dropwise to a solution of 200 mg of β-CD-MOFs in 20 ml of distilled water. The solution was stirred in dark at room temperature at 500 rpm for 2 h. 2 ml of ethanol was added to stop the reaction and the solution was stirred at the previous condition for another hour. The solution was freeze-dried and aldehyde-MOF was obtained [34].

#### 2.4.2. Glutamine- β-CD-MOF

100 mg of aldehyde-MOF was mixed with 10 ml of distilled water, and 50 mg of L-glutamine was added to it and stirred at 500 rpm at room temperature for 24 h. The solution was subsequently freeze-dried and glutamine-β-CD-MOF was obtained [34].

### 2.5. In situ fabrication of curcumin-loaded β-CD MOF (CCM-β-CD-MOF)

35 mg of curcumin was dissolved in 5 ml of MeOH and added to a solution containing 141.8 mg of β-CD and 56 mg of KOH. The solution was placed in the water bath at 50 °C for 6 h and was added to a solution of 56 mg of CTAB dissolved in 7 ml of methanol. The solution was kept overnight. The final product was obtained by centrifugation at 5000 rpm for 10 min followed by washing with ethanol and drying at room temperature.

### 2.6. Loading of curcumin into β-CD-MOF (β-CD-MOF@CCM), aldehyde-β-CD-MOF (aldehyde-β-CD-MOF@CCM), and glutamine-β-CD-MOF (glutamine-β-CD-MOF@CCM)

Curcumin post encapsulation into β-CD-MOF, aldehyde-β-CD-MOF, and glutamine-β-CD-MOF was carried out by the following procedure. Briefly, 6 mg of curcumin was dissolved in 3 ml of MeOH. Separately, different amounts (6,9,12,15,18 mg) of β-CD-MOF, aldehyde-β-CD-MOF, and glutamine-β-CD-MOF were added to the solution. The absorbance value of the solution was measured at 425 nm at regular time intervals (5 min and every hour afterward until the absorbance reading no longer changed) to determine the loading capacity of curcumin on the nanocarriers, based on the absorbance and the calibration curve of free curcumin. The drug-loaded particles were then centrifuged at 5000 rpm for 10 min and dried at room temperature for further use. The particles with the highest loading capacity percentage of curcumin were used for the experiments.

### 2.7. Loading capacity and encapsulation efficiency

The amount of curcumin that is not encapsulated in β-CD-MOF was calculated by measuring the remaining curcumin in the supernatant using a calibration curve obtained from an absorbance wavelength of 425 nm. The loading capacity (LC, %) and encapsulation efficiency (EE, %) were obtained using Equation (1) and Equation (2), respectively.

$$LC\ (\%) = \frac{Amount\ of\ encapsulated\ curcumin}{Total\ amount\ of\ nanocarrier\ after\ loading} \quad (1)$$

$$EE\ (\%) = \frac{Amount\ of\ encapsulated\ curcumin}{Total\ amount\ of\ curcumin} \times 100\% \quad (2)$$

### 2.8. Preparation of gelatin coating of β-CD-MOF (gelatin@β-CD-MOF)

To obtain gelatin-coated β-CD-MOF, a two-step dissolving procedure with the method described by Coester et al. was used with some modifications [35,36]. 10 ml of 5 % gelatin solution was prepared at 40 °C under gentle heating and constant stirring. After the solution was cooled down to room temperature, an equal volume of acetone was slowly added to the solution to dissolve gelatin and was kept for sedimentation. Subsequently, the supernatant was discarded and the sediment was re-dissolved in 10 ml of distilled water. Next, β-CD-MOFs@CCM containing the highest drug loading capacity was added to the solution. Then 10 ml of acetone was added until the mixture became turbid. The gelatin and nanocarriers were cross-linked using 300 μL of glutaraldehyde at room temperature overnight. Purification was done by three-fold centrifugation at 5000 rpm for 10 min and washed with (1:1 V/V) water: acetone solution. The same experiment was carried out without the addition of β-CD-MOFs@CCM and gelatin nanoparticles (GNPs) were obtained [36].

### 2.9. Drug release

The *in vitro* release profiles of curcumin were investigated in neutral (pH ~7.4) and acidic (pH ~5.5) mediums through the dialysis bag diffusion method [37]. Briefly, 5.5 mg of drug-loaded MOFs were dispersed in 3 ml of physiological buffer, PBS, at pH 7.4 and 5.5 for 5 min. Subsequently, bovine serum albumin (BSA) was added to achieve a final concentration of 1 mg $ml^{-1}$. The dispersion was transferred to a dialysis bag and placed in an Erlenmeyer flask containing 20 ml of PBS and kept at 37 ± 1 °C and shaken continuously at 120 rpm. Aliquots (2 ml) were withdrawn at different time intervals (5, 15, 30, 60, 90, 120 min, and hourly thereafter until 72 h) and replaced with fresh amounts of the buffer. After subsequent dilution, samples were analyzed using a UV–Visible spectrophotometer at 425 nm. The drug release from samples was calculated using Equation (3).

$$Drug\ release\ \% = \frac{C_f - C_0}{C_i} \quad (3)$$

In this equation, $C_f$ ($mg.ml^{-1}$) is the weight of the released drug into the solution from the nano-carriers at a given time, $C_0$ ($mg.ml^{-1}$) is the weight of the drug in the solution initially (at time 0), and $C_i$ is the weight of the loaded drug in nano-carriers. The weight of the drug released is obtained by measuring the absorbance of the drug and using a calibration curve of free drug in PBS to obtain it.

### 2.10. In vitro cytotoxicity

The anticancer activity of nano-carriers was studied through a cell viability study using an MTT assay [38]. MCF-7 (breast cancer cell line), AGS (human gastric cell line), and NIH/3T3 (normal cells, mouse embryonic fibroblast cell line) were used for cell viability experiments. All cell lines were cultured in Dulbecco's Modified Eagle Medium (DMEM) (Gibco, MT, USA) supplemented with 10 % heath-inactivated fetal bovine serum (FBS, Gibco, MT, USA) and 1 % penicillin/streptomycin (Gibco, MT, USA) at 37 °C under a humidified atmosphere containing 5 % $CO_2$. Cells were seeded at the density of $1 \times 10^4$ MCF, $1 \times 10^4$ AGS, $1.5 \times 10^4$ NIH/3T3 per well in 96-well plates overnight. The next day, the medium was replaced by 100 μl freshly prepared culture medium containing different concentrations of nanocarriers and incubated for 72 h in triplicate wells. After 72 h of incubation, cells were washed and incubated in a medium containing 10 μL of MTT solution (5.0 mg $ml^{-1}$). The plates were incubated for 4 h. Subsequently, the culture medium was removed, and the formazan crystals were dissolved with 100 μl of DMSO. The absorbance of viable cells and background control were measured at 570 and 630 nm by ELISA plate reader. The cell viability was calculated as the percentage inhibition in cell growth to the controls by using Equation (4).

$$viability = \frac{Sample\ absorbance - Blank\ absorbance}{Control\ absorbance - Blank\ zbsorbance} \times 100 \quad (4)$$

### 2.11. Statistical analysis

All measurements were conducted in triplicates and the data were represented as average ± standard deviation. The size of the synthesized nanoparticles is presented as an average ± standard deviation (n = 50). Dose-response curve analysis was performed using GraphPad Prism, version 6.07 software (San Diego, CA, USA). The results from three independent cell viability experiments were averaged and statistically analyzed using Student's t-test with the significance threshold at the level of $P < 0.05$.

## 3. Result and discussion

### 3.1. Characterization of β-CD-MOF

#### 3.1.1. X-ray diffraction

XRD is a useful technique for the investigation of the crystalline structure of CDs. CDs are crystalline materials possessing 'cage' or 'channel' type crystal structures. The commercially purchased CDs have cage-like structures with 'herring-bone' arrangements in which the cavity of each molecule is blocked by the adjacent molecule. In the channel structure, the CD molecules are aligned and stacked on top of each other, creating long cylindrical channels. Generally, the channel configuration of the CDs is the confirmation for the coordination [39].

Fig. S1 displays the XRD analysis results for β-CD-MOF and pristine β-CD, allowing for a comparison of their respective patterns. The XRD patterns of the β-CD-MOFs exhibited notable differences from those of the corresponding β-CD. Several peaks shifted, disappeared, or were replaced by new peaks. The primary diffraction peaks at 2θ of 4.5° and 8.95° in β-CD, corresponding to its cage-like structure, underwent significant changes. In Fig. S1, post β-CD-MOF synthesis, these peaks disappeared, and new peaks emerged at 2θ around ~17.45° and 18°. The narrow peak shapes indicated the materials possessed relatively high crystallinity. The distinctive peaks at 2θ of 6.45°, 9.25°, 12.3°, and 18.7° corresponded to β-CD-MOF crystal planes (200), (222), (330), and (630), respectively. The alterations in the XRD patterns provided clear evidence of interactions between CDs and K+ ions, leading to the formation of β-CD-MOF. These findings align with earlier literature reports that also described the formation of β-CD-MOF [40].

#### 3.1.2. 1H NMR

Nuclear magnetic resonance proved to be a precise technique for determining the formation of β-CD-MOF. The shift in hydrogen peaks, in comparison to the original β-CD peaks, demonstrated the MOF formation. In Fig. S2, the $^{1}$H NMR spectra for β-CD revealed doublet peaks at 5.74 and 5.76 ppm, corresponding to OH-2. The signals at 4.83 and 4.84 ppm were associated with H1 of β-CD. Additionally, a triplet signal at 4.46, 4.47, and 4.49 ppm corresponded to OH-6. The signals at 3.55, 3.58, 3.62, 3.64, 3.66, 3.67, 3.69, and 3.7 represented H5, H3, and H6. Finally, the signals at 3.31 and 3.33 corresponded to H2 and H4 [41]. In the β-CD-MOF structure, the intensity of the OH-2 signal at 5.74 and 5.76 decreased, indicating a reduction in hydroxyl groups that had formed bonds with potassium, with a few remaining in free form. Additionally, two new signals at 7.02 and 6.89 were observed, corresponding to the bond between hydroxyl groups attached to potassium.

#### 3.1.3. SEM

The scanning electron microscopy analysis was conducted to characterize the morphology and size of the prepared β-CD-MOF. Fig. S3 depicted the SEM image of β-CD-MOF, revealing uniform cubic shapes with a mean diameter of 301 ± 7 nm.

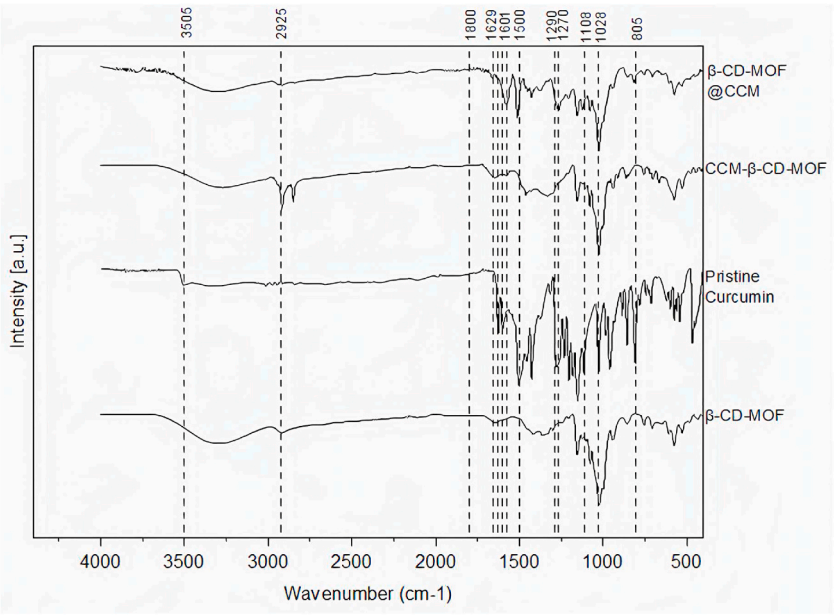


**Fig. 1.** FTIR spectrum of curcumin, β-CD-MOF, β-CD-MOF@CCM, and CCM-β-CD-MOF.

### 3.2. Characterization of the curcumin loaded β-CD-MOF

#### 3.2.1. XRD

The XRD patterns of curcumin, β-CD-MOF@CCM, and CCM-β-CD-MOF were presented in Fig. S4. Peaks corresponding to pristine curcumin were observed at 2θ of 8.95°, 17.3°, and within the 21-25° range, indicating the crystallinity of the drug. In β-CD-MOF@CCM, peaks related to both curcumin and β-CD-MOF were evident. Notably, the characteristic peak of curcumin at 17.3° was absent in the encapsulated structure, suggesting successful curcumin loading into the structure. Curcumin peaks were detected between 20 and 25° in the loaded structure, indicating some curcumin might have been physically adsorbed on the surface of the structures [25].In CCM-β-CD-MOF, the peaks corresponding to pristine curcumin at 8.95° and the characteristic peak at 17.3° were not observed. Furthermore, the curcumin peak at 21.2° exhibited a shift to 21.54° in the in situ synthesized structure. This shift strongly indicated the presence of curcumin in the β-CD-MOF from the early stages of synthesis [42].

#### 3.2.2. FTIR

The FTIR spectrum was acquired from curcumin, β-CD-MOF, β-CD-MOF@CCM, and CCM-β-CD-MOF, as depicted in Fig. 1. Notably, the prominent peak of curcumin at 3505 $cm^{-1}$, representing the hydroxyl (phenolic) vibration, was not observed in the spectrum of curcumin-loaded β-CD-MOF. This absence strongly indicated the formation of hydrogen bonds between the phenolic hydroxyl groups of curcumin and the hydroxyl group of β-CD-MOF [25]. In the spectrum of curcumin, no bands were detected in the carbonyl region of 1620–1800 $cm^{-1}$. This absence signifies that curcumin is present in the keto-enol tautomeric form, known for its higher bioactivity [42]. The stretching vibration of C═O and C═C at 1626 $cm^{-1}$ in the aromatic ring experienced a shift to 1653 $cm^{-1}$. This shift indicated that both benzene rings of curcumin were enclosed within the β-CD-MOF through van der Waals forces and hydrophobic interactions. Moreover, the peak at 1270 $cm^{-1}$ in curcumin shifted to 1290 $cm^{-1}$ in the loaded structure, suggesting an interaction between β-CD-MOF and the ring on the enolic side of the curcumin molecule. Additionally, the stretching of aromatic rings at 1601 $cm^{-1}$ in the curcumin structure shifted to 1574 $cm^{-1}$ in the loaded particles [42,43].

#### 3.2.3. SEM

In Fig. S5, the SEM images of CCM-β-CD-MOF and β-CD-MOF@CCM were presented. Both sets of particles distinctly maintained their cubic structures, illustrating the robustness of the MOF framework under varying loading conditions. An interesting observation is that CCM-β-CD-MOF potentially has curcumin adsorbed on its surface, which could contribute to the observed structural differences.

### 3.3. Characterization of glutamine-β-CD-MOF

#### 3.3.1. $^1H$ NMR

Before functionalization with L-glutamine, the hydroxyl groups underwent oxidation to aldehydes. Since hydroxyl and amine groups do not readily react due to their nucleophilic nature, oxidation of the hydroxyl groups was essential to form aldehydes. Fig. 2 illustrates the $^1H$ NMR of aldehyde-β-CD-MOF, displaying a distinct peak at 8.13 ppm, signifying the successful formation of aldehyde groups. The signal corresponding to OH-2 in β-CD-MOF (Fig. S2) vanished, indicating the reduction of hydroxyl groups.

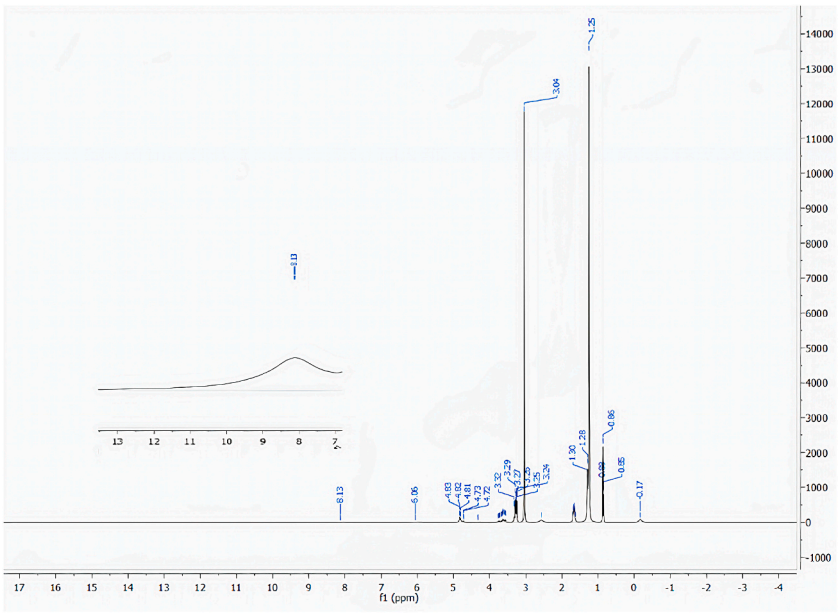


**Fig. 2.** $^1H$ NMR of aldehyde-β-CD-MOF

### 3.3.2. FTIR

The FTIR spectra of glutamine-β-CD-MOF in Fig. 3 demonstrated a double peak at 3400 $cm^{-1}$ corresponding to the stretching vibration of the N–H bond which overlaps with the O–H signal. This region often encompasses both N–H and O–H stretching vibrations, and the presence of glutamine in the sample can lead to the overlapping of these signals, resulting in a double peak or broadening in this region. The peak at 2935 $cm^{-1}$ correlated to the C–H stretching vibrations. Signals at 1630 $cm^{-1}$ and 1546 $cm^{-1}$ corresponded to C═O and C–N vibrations, respectively. The FTIR peak at approximately 1500 $cm^{-1}$ was associated with the bending vibrations of the amine ($NH_2$) group. This region is known as the "amide II" band and is characteristic of proteins and peptides which contain amine functionalities. The vibration of C–O was observed at 1439 $cm^{-1}$. The out-of-plane vibration of the N–H bond was present at 730 $cm^{-1}$ and 670 $cm^{-1}$. After functionalization with L-glutamine, the characteristic peak of OH in β-CD-MOF at 3300 $cm^{-1}$ has reduced. The vibration of the C–C bond was observed at 853 $cm^{-1}$. The signal at 1028 $cm^{-1}$ and 1081 $cm^{-1}$ correlated to the C–O bond. The bonds correlating to the structure of β-CD-MOF and bonds correlating to the formation of N–H bonds indicated the successful functionalization and formation of glutamine-β-CD-MOF.

### 3.3.3. XRD

The XRD analysis of glutamine-β-CD-MOF is presented in Fig. S6. Peaks at 2θ of 23.55° and 25.45° were attributed to L-glutamine, clearly indicating its presence. Concurrently, the β-CD-MOF peaks observed at 12°, 17°, and 18° were consistent with the pristine β-CD-MOF. The XRD pattern of glutamine-β-CD-MOF vividly displayed peaks corresponding to both L-glutamine and β-CD-MOF, affirming successful functionalization of the structures.

### 3.3.4. SEM

The SEM image of glutamine-β-CD-MOF is illustrated in Fig. S7. Notably, the morphology of the structure remained unaltered even after functionalization with L-glutamine, indicating the robustness and stability of the MOF structure.

## 3.4. Characterization of gelatin@β-CD-MOF

### 3.4.1. FTIR

In Fig. 4, the FTIR spectra of pure gelatin, gelatin nanoparticles (GNPs), and gelatin@β-CD-MOF are presented. The GNPs were generated using a two-step desolvation method and subsequently cross-linked with glutaraldehyde. This crosslinking process has induced changes in the spectra, resulting in noticeable differences between GNPs and gelatin. Intriguingly, the gelatin@β-CD-MOF showcases spectra akin to that of GNPs, indicating successful coating of the MOF structure by gelatin.

### 3.4.2. XRD

In Fig. S8, the XRD patterns of β-CD-MOF and gelatin@β-CD-MOF are illustrated. It's important to note that gelatin possesses an amorphous structure. Consequently, the coating process with gelatin resulted in the development of an amorphous structure, as depicted in the XRD pattern.

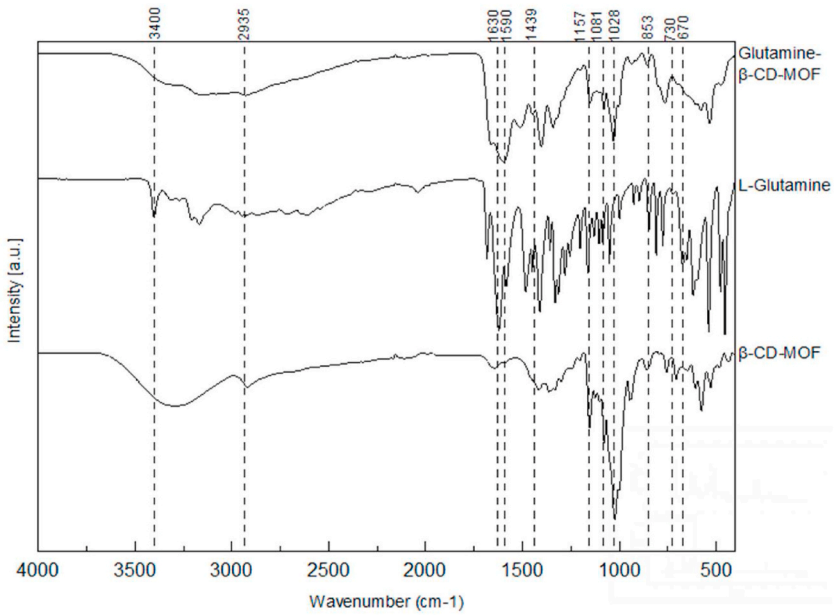


**Fig. 3.** FTIR spectra of glutamine-β-CD-MOF, glutamine, and β-CD-MOF.

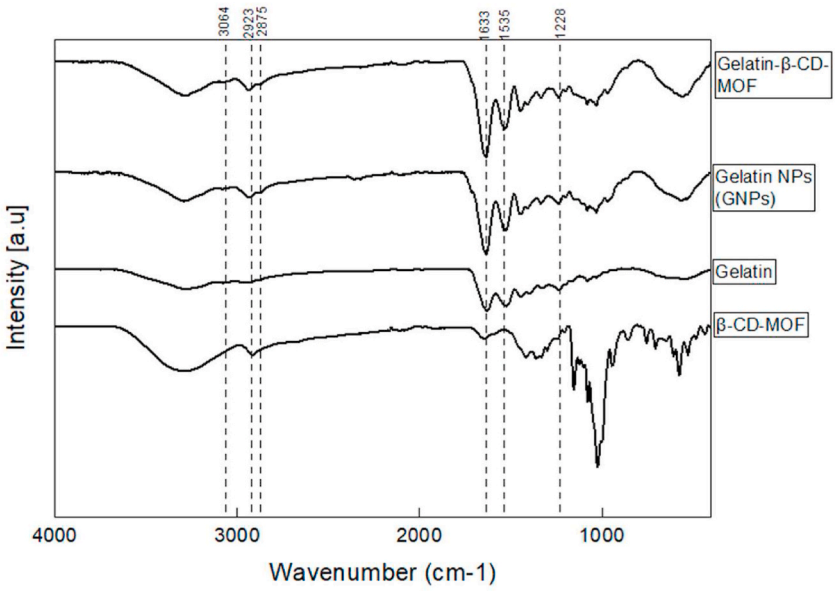


**Fig. 4.** FTIR spectra of pure gelatin, GNPs, and gelatin@β-CD-MOF

### *3.4.3. SEM*

The SEM image of gelatin@β-CD-MOF depicted in Fig. S9 highlights a distinctive spherical morphology with an average size of 293 ± 5 nm. This spherical structure strongly supports the successful gelatin coating, inducing notable changes in the overall structures. It's noteworthy that the average size of gelatin@β-CD-MOF is observed to be smaller compared to pristine β-CD-MOF. This reduction in size can be attributed to the presence of gelatin, a biopolymer that generates steric hindrance, effectively impeding particle

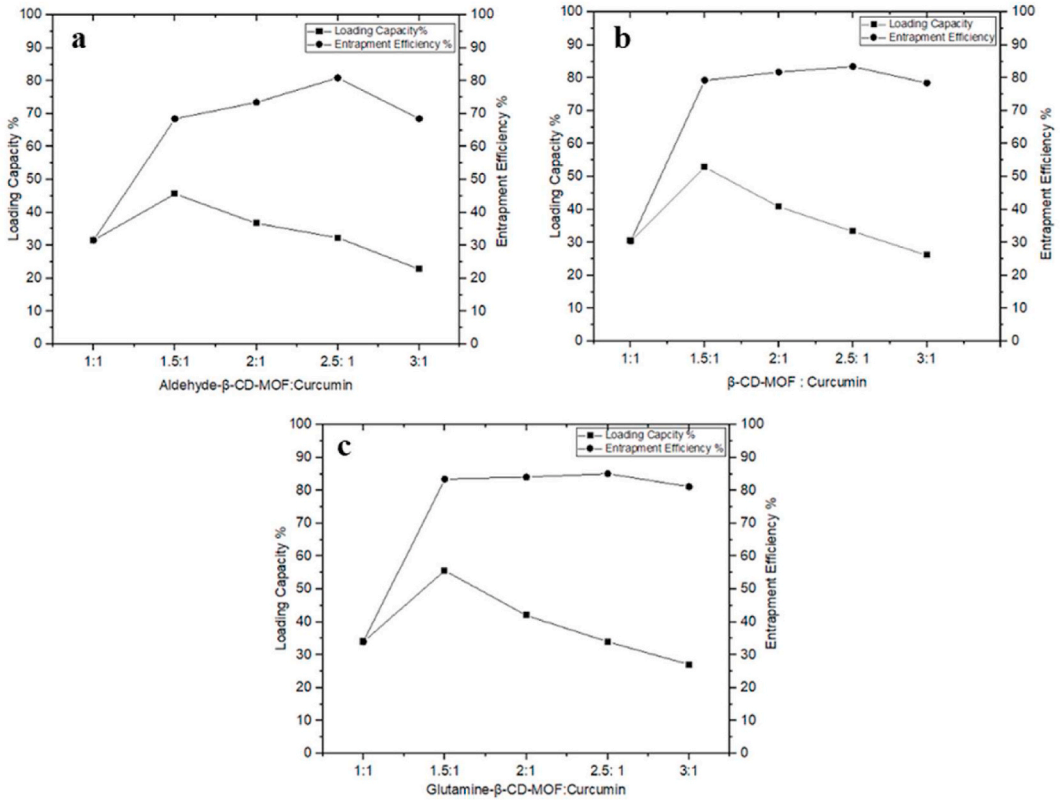


**Fig. 5.** Loading capacity for a) aldehyde-β-CD-MOF@CCM, b) β-CD-MOF@CCM, and c) glutamine- β-CD-MOF@CCM

aggregation and agglomeration, thus resulting in a smaller size.

### 3.5. Drug loading capacity and efficiency

In this study, post-encapsulated curcumin-loaded β-CD-MOF (β-CD-MOF@CCM) was prepared using different mass ratios (1:1, 1:1.5, 2:1, 2.5:1, 3:1) of curcumin to β-CD-MOF. The optimal loading capacity was determined at the mass ratio of 1:1.5 for all nanocarriers. Fig. 5 illustrates that the highest loading capacity achieved for β-CD-MOF@CCM, aldehyde-β-CD-MOF@CCM, and glutamine- β-CD-MOF@CCM was 52.38 %, 45.4 %, and 55.63 %, respectively. Furthermore, the encapsulation efficiency for β-CD-MOF@CCM, aldehyde-β-CD-MOF@CCM, and glutamine-β-CD-MOF@CCM stood at 79.24 %, 68.47 %, and 83.45 %, respectively. Notably, the loading capacity of aldehyde-β-CD-MOF was slightly lower than that of β-CD-MOF, attributable to the oxidation of hydroxyl groups to aldehydes during functionalization. The phenolic groups in curcumin have an affinity for hydroxyl groups, consequently, a decrease in the number of hydroxyl groups results in a reduced loading capacity. Conversely, the loading capacity of glutamine-β-CD-MOF increased due to curcumin's high affinity towards the amine functional groups in glutamine. Earlier studies reported the loading capacity of β-CD-MOF for Emodin and Quercetin as 142.2 mg $g^{-1}$ and 196.4 mg $g^{-1}$ [33,40].

Furthermore, the encapsulation efficiency of menthol in β-CD-MOF was obtained to be 22.54 %. In another study, the loading capacity of dimercaptosuccinic acid in β-CD-MOF was obtained to be 12.17 % [44]. The anti-inflammatory ibuprofen had a loading capacity of 7.3 wt % in β-CD-MOF [45]. The β-CD has also been previously utilized for drug delivery of curcumin but had a loading efficiency of 32.17 % which is lower than the loading efficiency of β-CD-MOF in this study [46]. This can be attributed to the higher porosity and larger surface area (1123 $m^2/g$) of β-CD-MOF [47].

According to Fig. S10 the absorbance of curcumin in the supernatant solution reduced over time, indicating successful loading of the drug inside β-CD-MOF.

Fig. S11 demonstrates the loading of the drug curcumin into nano-carries as a function of time. In the initial stages, loading had a higher rate which was attributed to the available sites, then slowed down and reached equilibrium after 24 h.

### 3.6. Drug release

The acidic microenvironment, characterized by pH values ranging from 5.6 to 6.8 in malignant tumor cells, was primarily attributed to the prevalence of the glycolysis pathway in cancer cells. Hypoxia, resulting from irregular angiogenesis, further contributed to this acidic milieu. Conversely, in normal tissues, the Krebs pathway held dominance, and the presence of oxygen inhibited glycolysis, maintaining a neutral pH in the microenvironment [48]. The *in vitro* drug release profile of curcumin from nano-carriers was depicted as the cumulative percentage of released drugs over time. Drug release monitoring occurred at both pH 7.4 and 5.5 for a duration of 72 h. This pH range was selected to illustrate the impact of physiological and acidic pH values on drug release. Given that cancer cells tend to acidify their extracellular environment, an optimal carrier should exhibit higher release rates within this acidic range.

Fig. 6a presents the release profiles of curcumin from various carriers in pH 7.4 PBS. The release percentages for β-CD-MOF@CCM, CCM-β-CD-MOF, glutamine-β-CD-MOF@CCM, and gelatin@β-CD-MOF@CCM at pH 7.4 were 13.12 %, 11.94 %, 8.68 %, and 9.24 %, respectively. The distinct release rates stem from the encapsulation methods employed. Post-encapsulation resulted in a higher release rate, attributed to surface adsorption of curcumin onto the nanocarriers. Conversely, in situ encapsulated curcumin exhibited a slower release, facilitated by its location within the structure and hydrogen bonding with hydroxyl groups of β-CD-MOFs, as confirmed by FTIR analysis. Gelatin coating, known for its stability in neutral pH, yielded a controlled release pattern over 72 h. The reduced release rate from glutamine-functionalized structures is attributed to the strong affinity between glutamine's amine groups and curcumin's phenol groups.

Fig. 6b displays the curcumin release profiles at pH 5.5. Curcumin release from β-CD-MOF@CCM, CCM-β-CD-MOF, glutamine-β-CD-MOF@CCM, and gelatin@β-CD-MOF@CCM at pH 5.5 was 74.46 %, 69.53 %, 62.14 %, and 55.98 %, respectively. Structures coated with gelatin and functionalized with glutamine exhibited slower release rates, likely due to amine groups deprotonating in the

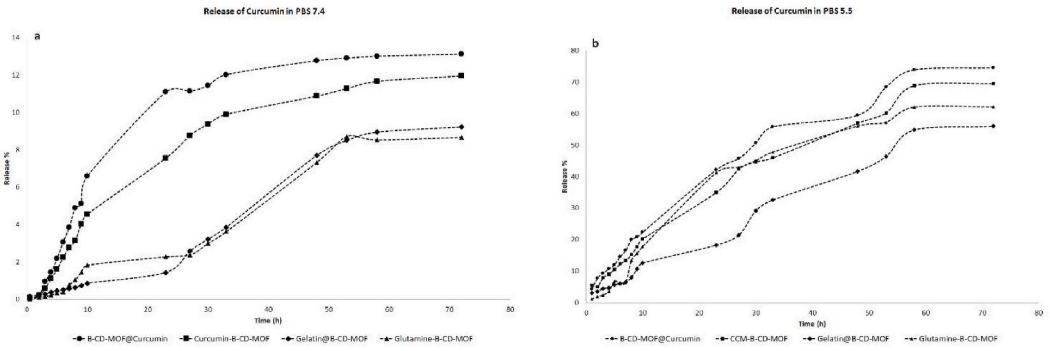


**Fig. 6.** a) Curcumin release in PBS 7.4 and b) Curcumin release in PBS 5.5.

acidic pH, delaying drug release. The gelatin coating demonstrated sensitivity to an acidic environment, acting as a protective barrier. Upon exposure to the acidic environment, which typically triggers faster release, the gelatin coating impeded the penetration of the acidic medium into the MOF structure, thereby reducing the rate of curcumin release. Subsequent coating degradation exposed the structure to an acidic environment, facilitating drug release.

As anticipated, a lower drug release was observed at pH 7.4, attributed to the stability of the particles in this neutral medium. This observation holds paramount importance, given that the physiological pH of healthy cells is approximately 7.4. Conversely, at the lower pH of 5.5, the drug exhibited a faster release. Notably, functionalized particles with glutamine and gelatin-coated structures showcased reduced burst release and a more controlled, sustained release profile.

### 3.7. Cytotoxicity

Figs. 7 and 8 showcased the MTT assays conducted on three distinct cell lines: MCF-7, AGS, and NIH/3T3, following a 72-h incubation period. Fig. 7 provided insights from the MTT assay for β-CD-MOF@CCM, glutamine- β-CD-MOF@CCM, and CCM-β-CD-MOF, encompassing concentrations ranging from 12.5 to 200 μg $ml^{-1}$. On the other hand, Fig. 8 illustrated the MTT assay results for gelatin@β-CD-MOF and gelatin@β-CD-MOF@CCM within the concentration range of 12.5–300 μg $ml^{-1}$.

In Fig. 7, the cellular viability of β-CD-MOF@CCM dipped below 80 % at concentrations exceeding 100 μg $ml^{-1}$. Specifically, at 100 μg $ml^{-1}$, the cell viability for NIH/3T3, MCF-7, and AGS decreased to 54.34 %, 64.92 %, and 37.3 %, respectively. Similarly, at 200 μg $ml^{-1}$, the cell viability for NIH/3T3, MCF-7, and AGS plummeted to 42.67 %, 42.63 %, and 16.15 %, respectively. For CCM-β-CD-MOF, the cellular viability dropped below 80 % at 200 μg $ml^{-1}$, revealing respective viabilities of 51.85 %, 54 %, and 11.92 % for NIH/3T3, MCF-7, and AGS at the same concentration. Furthermore, the cell viability for glutamine-β-CD-MOF@CCM decreased to less than 80 % at concentrations surpassing 100 μg $ml^{-1}$. At 100 μg $ml^{-1}$, cellular viability for NIH/3T3, MCF-7, and AGS stood at 80.14 %, 26.77 %, and 37.69 %, respectively. At 200 μg $ml^{-1}$, the cell viability for NIH/3T3, MCF-7, and AGS registered as 54.9 %, 17.89 %, and 18.07 %, respectively. Notably, glutamine-β-CD-MOF@CCM exhibited higher specificity in reducing the viability of MCF-7 and AGS compared to NIH/3T3, while structures without glutamine displayed heightened cytotoxicity towards fibroblast cells. The results affirm that β-CD-MOF and glutamine-β-CD-MOF are non-toxic and safe for drug delivery. Immobilization of L-glutamine for capturing cancer cells resulted in greater cancer cell toxicity compared to normal cell toxicity.

In Fig. 8, gelatin@β-CD-MOF exhibited viability lower than 80 % at concentrations exceeding 200 μg $ml^{-1}$ for NIH/3T3 cells. Specifically, the cell viability for NIH/3T3 cells reduced to 77.27 % and 70.66 % at 200 and 300 μg $ml^{-1}$, respectively. Likewise, for MCF-7 cells, cellular viability dropped below 80 % at gelatin@β-CD-MOF concentrations exceeding 100 μg $ml^{-1}$. At concentrations of 100, 200, and 300 μg $ml^{-1}$, the cell viability for MCF-7 cells stood at 77.91 %, 76.6 %, and 75.73 %, respectively. At a concentration of 300 μg $ml^{-1}$ of gelatin@β-CD-MOF, the cellular viability for AGS cells decreased to 65.77 %. The cell viability of NIH/3T3 cells for gelatin@β-CD-MOF@CCM fell below 80 % at concentrations of 200 and 300 μg $ml^{-1}$. Specifically, at 200 μg $ml^{-1}$ and 300 μg $ml^{-1}$, the viability dropped to 64.66 % and 45.14 %, respectively. The MCF-7 cell viability for gelatin@β-CD-MOF@CCM dipped below 80 % for concentrations exceeding 100 μg $ml^{-1}$. Specifically, at 100, 200, and 300 μg $ml^{-1}$, the cellular viability of MCF-7 for gelatin@β-CD-MOF@CCM reduced to 37.97 %, 16.97 %, and 10.44 %, respectively. For AGS cells, the viability decreased to 31.01 % and 20.64 % at 200 μg $ml^{-1}$ and 300 μg $ml^{-1}$ of gelatin@β-CD-MOF@CCM. Comparatively, the cellular viability of drug-loaded structures, gelatin@β-CD-MOF@CCM, was significantly lower compared to gelatin@β-CD-MOF. This underscored the effectiveness of the loaded structure for targeting cancer cells.

## 4. Conclusion

In conclusion, this study successfully developed functionalized encapsulated systems for efficient hydrophobic drug delivery. The biocompatible β-CD-MOF was synthesized using a modified vapor diffusion method. The β-CD-MOF was innovatively coated and functionalized with gelatin and L-glutamine, presenting novel approaches. L-glutamine, a crucial component in cancer cell metabolism, was employed to specifically target cancer cells, underlining the potential of glutamine-β-CD-MOF for further functionalization. Oxidation of outer hydroxyl groups to aldehydes allowed for unique reactivity with amino groups. The loading capacities of β-CD-MOF@CCM, CCM-β-CD-MOF, and glutamine-β-CD-MOF@CCM were notably high, especially at the 1:1.5 ratio of curcumin:nanocarrier. Controlled drug release over 72 h was observed in the coated and functionalized structures. Glutamine functionalization demonstrated enhanced specificity for cancer cells, a critical advantage. Furthermore, the biocompatible gelatin coating, particularly in gelatin@β-CD-MOF, significantly reduced cancer cell viability. These functionalized β-CD MOFs offer promising advantages, including high drug loading capacity, controlled drug release, cancer cell-specific targeting, and versatile modification potential. Moreover, the use of biocompatible gelatin coating ensures safe and biocompatible drug delivery systems, highlighting their potential in targeted drug delivery, especially in cancer therapy and related fields.

## CRediT authorship contribution statement

**Pegah Sadeh:** Writing – original draft, Visualization, Validation, Formal analysis, Data curation. **Sedigheh Zeinali:** Writing – review & editing, Supervision, Project administration, Methodology, Funding acquisition. **Banafsheh Rastegari:** Writing – review & editing, Supervision, Project administration. **Iman Najafipour:** Writing – original draft, Investigation, Data curation.

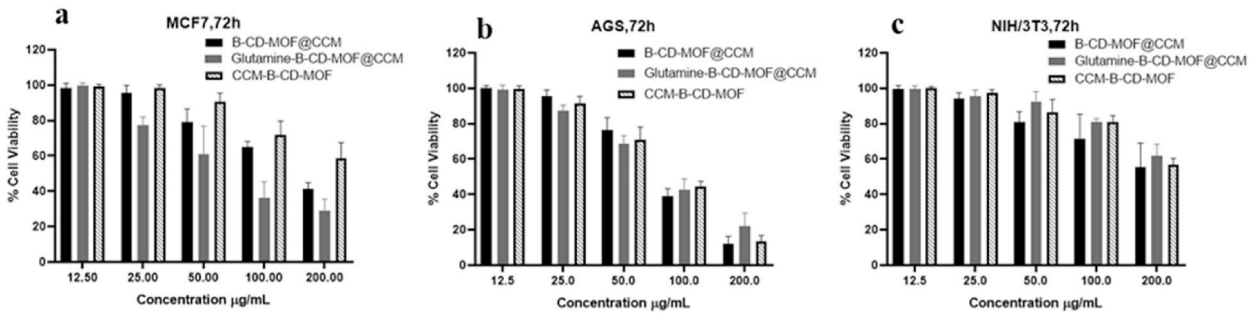


**Fig. 7.** Cell viability of β-CD-MOF@CCM, glutamine-β-CD-MOF@CCM, and CCM-β-CD-MOF in a) MCF, b) AGS, and c) NIH/3T3 for 72h

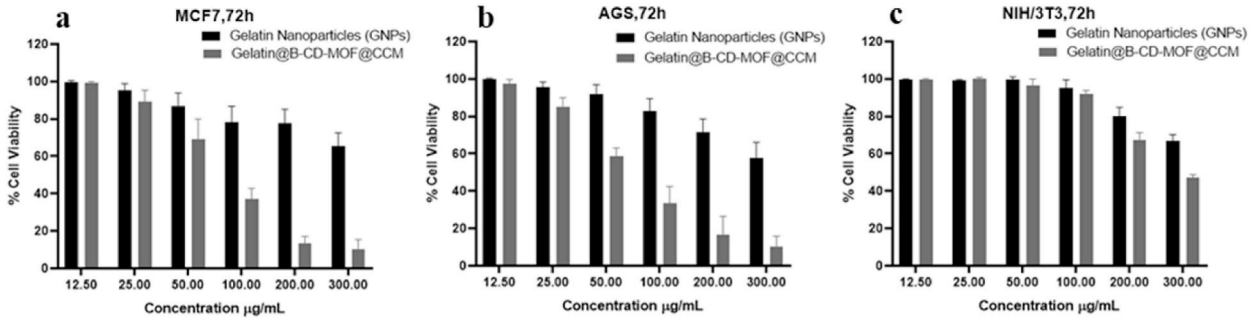


**Fig. 8.** Cell viability and cytotoxicity of GNPs, and Gelatin-β-CD-MOF@CCM in a) MCF, b) AGS, and c) NIH/3T3 for 72h

## Declaration of competing interest

The authors declare that they have no known competing financial interests or personal relationships that could have appeared to influence the work reported in this paper.

## Acknowledgment

This research was supported by the Department of Nonchemical Engineering and Nanotechnology Research Institute of Shiraz University.

## Appendix A. Supplementary data

Supplementary data to this article can be found online at https://doi.org/10.1016/j.heliyon.2024.e30349.

## References

[1] A. Abbasi Kajani, S. Haghjooy Javanmard, M. Asadnia, A. Razmjou, Recent advances in nanomaterials development for nanomedicine and cancer, ACS Appl. Bio Mater. 4 (2021) 5908–5925, https://doi.org/10.1021/acsabm.1c00591.
[2] T.A. Vahed, M.R. Naimi-Jamal, L. Panahi, Alginate-coated ZIF-8 metal-organic framework as a green and bioactive platform for controlled drug release, J. Drug Deliv. Sci. Technol. 49 (2019) 570–576, https://doi.org/10.1016/j.jddst.2018.12.022.
[3] S. Keskin, S. Kızılel, Biomedical applications of metal organic frameworks, Ind. Eng. Chem. Res. 50 (2011) 1799–1812, https://doi.org/10.1021/ie101312k.
[4] C. Pettinari, F. Marchetti, N. Mosca, G. Tosi, A. Drozdov, Application of metal− organic frameworks, Polym. Int. 66 (2017) 731–744, https://doi.org/10.1002/pi.5315.
[5] R. Ricco, C. Pfeiffer, K. Sumida, C.J. Sumby, P. Falcaro, S. Furukawa, N.R. Champness, C.J. Doonan, Emerging applications of metal–organic frameworks, CrystEngComm 18 (2016) 6532–6542, https://doi.org/10.1039/C6CE01030J.
[6] J. Yang, Y.W. Yang, Metal–organic frameworks for biomedical applications, Small 16 (2020) 1906846, https://doi.org/10.1002/smll.201906846.
[7] T. Rajkumar, D. Kukkar, K.-H. Kim, J.R. Sohn, A. Deep, Cyclodextrin-metal–organic framework (CD-MOF): from synthesis to applications, J. Ind. Eng. Chem. 72 (2019) 50–66, https://doi.org/10.1016/j.jiec.2018.12.048.
[8] F. Mokhtarian, B. Rastegari, S. Zeinali, M. Tohidi, H.R. Karbalaei-Heidari, Theranostic effect of folic acid functionalized MIL-100 (Fe) for delivery of prodigiosin and simultaneous tracking-combating breast cancer, J. Nanomater. 2022 (2022), https://doi.org/10.1155/2022/1108865.
[9] M. Ghanbarian, S. Zeinali, A. Mostafavi, T. Shamspur, Facile synthesis of MIL-53 (Fe) by microwave irradiation and its application for robust removal of heavy metals from aqueous solution by experimental design approach: kinetic and equilibrium, Anal. Bioanal. Chem. Res. 7 (2020) 263–280, https://doi.org/10.22036/abcr.2019.172731.1319.

[10] J. Shadmehr, S. Zeinali, M. Tohidi, Synthesis of a chromium terephthalate metal organic framework and use as nanoporous adsorbent for removal of diazinon organophosphorus insecticide from aqueous media, J. Dispersion Sci. Technol. (2019), https://doi.org/10.1080/01932691.2018.1516149.
[11] M. Hosseini, S. Zeinali, Capacitive humidity sensing using a metal–organic framework nanoporous thin film fabricated through electrochemical in situ growth, J. Mater. Sci. Mater. Electron. 30 (2019) 3701–3710, https://doi.org/10.1007/s10854-018-00652-8.
[12] D. Yang, B.C. Gates, Catalysis by metal organic frameworks: perspective and suggestions for future research, ACS Catal. 9 (2019) 1779–1798, https://doi.org/10.1021/acscatal.8b04515.
[13] F.D. Duman, R.S. Forgan, Applications of nanoscale metal–organic frameworks as imaging agents in biology and medicine, J. Mater. Chem. B 9 (2021) 3423–3449, https://doi.org/10.1039/D1TB00358E.
[14] D.Y. Lee, D.V. Shinde, S.J. Yoon, K.N. Cho, W. Lee, N.K. Shrestha, S.-H. Han, Cu-based metal–organic frameworks for photovoltaic application, J. Phys. Chem. C 118 (2014) 16328–16334, https://doi.org/10.1021/jp4079663.
[15] H. Furukawa, K.E. Cordova, M. O'Keeffe, O.M. Yaghi, The chemistry and applications of metal-organic frameworks, Science 341 (2013) 1230444, https://doi.org/10.1126/science.1230444.
[16] J. Liu, A. Bahadoran, N. Emami, T.J. Al-Musawi, F.A. Dawood, N. Nasajpour-Esfahani, I. Najafipour, S.E. Mousavi, T. Ghazuan, M. Mosallanezhad, Removal of diclofenac sodium and cefixime from wastewater by polymeric PES mixed-matrix-membranes embedded with MIL101-OH/Chitosan, Process Saf. Environ. Protect. 172 (2023) 588–593, https://doi.org/10.1016/j.psep.2023.02.060.
[17] Z. Liu, A. Bahadoran, A.a. Alizadeh, N. Emami, T.J. Al-Musaw, A.H.R. Alawadi, A.M. Aljeboree, M. Shamsborhan, I. Najafipour, S.E. Mousavi, Sonocrystallization of a novel ZIF/zeolite composite adsorbent with high chemical stability for removal of the pharmaceutical pollutant azithromycin from contaminated water, Ultrason. Sonochem. 97 (2023) 106463, https://doi.org/10.1016/j.ultsonch.2023.106463.
[18] M.P. Abuçafy, B.L. Caetano, B.G. Chiari-Andréo, B. Fonseca-Santos, A.M. do Santos, M. Chorilli, L.A. Chiavacci, Supramolecular cyclodextrin-based metal-organic frameworks as efficient carrier for anti-inflammatory drugs, Eur. J. Pharm. Biopharm. 127 (2018) 112–119, https://doi.org/10.1016/j.ejpb.2018.02.009.
[19] B. Sun, M. Bilal, S. Jia, Y. Jiang, J. Cui, Design and bio-applications of biological metal-organic frameworks, Kor. J. Chem. Eng. 36 (2019) 1949–1964, https://doi.org/10.1007/s11814-019-0394-8.
[20] S.L. Anderson, K.C. Stylianou, Biologically derived metal organic frameworks, Coord. Chem. Rev. 349 (2017) 102–128, https://doi.org/10.1016/j.ccr.2017.07.012.
[21] J. Qiu, X. Li, R. Gref, A. Vargas-Berenguel, Carbohydrates in metal organic frameworks: supramolecular assembly and surface modification for biomedical applications, in: Metal-Organic Frameworks for Biomedical Applications, Elsevier, 2020, pp. 445–465.
[22] H. Cai, Y.-L. Huang, D. Li, Biological metal–organic frameworks: structures, host–guest chemistry and bio-applications, Coord. Chem. Rev. 378 (2019) 207–221, https://doi.org/10.1016/j.ccr.2017.12.003.
[23] J.-Q. Sha, L.-H. Wu, S.-X. Li, X.-N. Yang, Y. Zhang, Q.-N. Zhang, P.-P. Zhu, Synthesis and structure of new carbohydrate metal–organic frameworks and inclusion complexes, J. Mol. Struct. 1101 (2015) 14–20, https://doi.org/10.1016/j.molstruc.2015.08.020.
[24] P. George, R.K. Das, P. Chowdhury, Facile microwave synthesis of Ca-BDC metal organic framework for adsorption and controlled release of Curcumin, Microporous Mesoporous Mater. 281 (2019) 161–171, https://doi.org/10.1016/j.micromeso.2019.02.028.
[25] Z. Moussa, M. Hmadeh, M.G. Abiad, O.H. Dib, D. Patra, Encapsulation of curcumin in cyclodextrin-metal organic frameworks: dissociation of loaded CD-MOFs enhances stability of curcumin, Food Chem. 212 (2016) 485–494, https://doi.org/10.1016/j.foodchem.2016.06.013.
[26] M. Moballegh Nasery, B. Abadi, D. Poormoghadam, A. Zarrabi, P. Keyhanvar, H. Khanbabaei, M. Ashrafizadeh, R. Mohammadinejad, S. Tavakol, G. Sethi, Curcumin delivery mediated by bio-based nanoparticles: a review, Molecules 25 (2020) 689, https://doi.org/10.3390/molecules25030689.
[27] M.M. Yallapu, M. Jaggi, S.C. Chauhan, β-Cyclodextrin-curcumin self-assembly enhances curcumin delivery in prostate cancer cells, Colloids Surf. B Biointerfaces 79 (2010) 113–125, https://doi.org/10.1016/j.colsurfb.2010.03.039.
[28] C.S. Mangolim, C. Moriwaki, A.C. Nogueira, F. Sato, M.L. Baesso, A.M. Neto, G. Matioli, Curcumin–β-cyclodextrin inclusion complex: stability, solubility, characterisation by FT-IR, FT-Raman, X-ray diffraction and photoacoustic spectroscopy, and food application, Food Chem. 153 (2014) 361–370, https://doi.org/10.1016/j.foodchem.2013.12.067.
[29] V.J. Stella, Q. He, Cyclodextrins, Toxicol. Pathol. 36 (2008) 30–42, https://doi.org/10.1177/0192623307310945.
[30] X. Huang, C.S. Brazel, On the importance and mechanisms of burst release in matrix-controlled drug delivery systems, J. Contr. Release 73 (2001) 121–136, https://doi.org/10.1016/S0168-3659(01)00248-6.
[31] A. Arun, P. Malrautu, A. Laha, S. Ramakrishna, Gelatin nanofibers in drug delivery systems and tissue engineering, Eng. Sci. 16 (2021) 71–81, https://doi.org/10.30919/es8d527.
[32] C.T. Hensley, A.T. Wasti, R.J. DeBerardinis, Glutamine and cancer: cell biology, physiology, and clinical opportunities, J. Clin. Invest. 123 (2013) 3678–3684, https://doi.org/10.1172/JCI69600.
[33] A. Yang, H. Liu, Z. Li, L. Li, W. Li, K. Liu, Green synthesis of β-cyclodextrin metal–organic frameworks and the adsorption of quercetin and emodin, Polyhedron 159 (2019) 116–126, https://doi.org/10.1016/j.poly.2018.11.043.
[34] W. Fan, Y. Xu, Z. Li, Q. Li, Folic acid-modified β-cyclodextrin nanoparticles as drug delivery to load DOX for liver cancer therapeutics, Soft Mater. 17 (2019) 437–447, https://doi.org/10.1080/1539445X.2019.1624265.
[35] Y. Wang, H. Chen, C. Ye, Y. Hu, Synthesis and characterization of CdTe quantum dots embedded gelatin nanoparticles via a two-step desolvation method, Mater. Lett. 62 (2008) 3382–3384, https://doi.org/10.1016/j.matlet.2008.03.039.
[36] C. Coester, K. Langer, H. Von Briesen, J. Kreuter, Gelatin nanoparticles by two step desolvation a new preparation method, surface modifications and cell uptake, J. Microencapsul. 17 (2000) 187–193, https://doi.org/10.1080/026520400288427.
[37] S. Bohrey, V. Chourasiya, A. Pandey, Polymeric nanoparticles containing diazepam: preparation, optimization, characterization, in-vitro drug release and release kinetic study, Nano Converg 3 (2016) 1–7, https://doi.org/10.1186/s40580-016-0061-2.
[38] T. Mosmann, Rapid colorimetric assay for cellular growth and survival: application to proliferation and cytotoxicity assays, J. Immunol. Methods 65 (1983) 55–63, https://doi.org/10.1016/0022-1759(83)90303-4.
[39] T. Uyar, Y. Nur, J. Hacaloglu, F. Besenbacher, Electrospinning of functional poly (methyl methacrylate) nanofibers containing cyclodextrin-menthol inclusion complexes, Nanotechnology 20 (2009) 125703, https://doi.org/10.1088/0957-4484/20/12/125703.
[40] Z. Hu, S. Li, S. Wang, B. Zhang, Q. Huang, Encapsulation of menthol into cyclodextrin metal-organic frameworks: preparation, structure characterization and evaluation of complexing capacity, Food Chem. 338 (2021) 127839, https://doi.org/10.1016/j.foodchem.2020.127839.
[41] M. Raoov, S. Mohamad, M.R. Abas, Synthesis and characterization of β-cyclodextrin functionalized ionic liquid polymer as a macroporous material for the removal of phenols and as (V), Int. J. Mol. Sci. 15 (2013) 100–119, https://doi.org/10.3390/ijms15010100.
[42] Y. Chen, K. Tai, P. Ma, J. Su, W. Dong, Y. Gao, L. Mao, J. Liu, F. Yuan, Novel γ-cyclodextrin-metal–organic frameworks for encapsulation of curcumin with improved loading capacity, physicochemical stability and controlled release properties, Food Chem. 347 (2021) 128978, https://doi.org/10.1016/j.foodchem.2020.128978.
[43] T.M. Kolev, E.A. Velcheva, B.A. Stamboliyska, M. Spiteller, DFT and experimental studies of the structure and vibrational spectra of curcumin, Int. J. Quant. Chem. 102 (2005) 1069–1079, https://doi.org/10.1002/qua.20469.
[44] Y. Xiong, L. Wu, T. Guo, C. Wang, W. Wu, Y. Tang, T. Xiong, Y. Zhou, W. Zhu, J. Zhang, Crystal transformation of β-CD-MOF facilitates loading of dimercaptosuccinic acid, AAPS PharmSciTech 20 (2019) 1–9, https://doi.org/10.1208/s12249-019-1422-z.
[45] T. Volkova, A. Surov, I. Terekhova, Metal–organic frameworks based on β-cyclodextrin: design and selective entrapment of non-steroidal anti-inflammatory drugs, J. Mater. Sci. 55 (2020) 13193–13205, https://doi.org/10.1007/s10853-020-04937-4.

[46] C.-H. Liu, G.-W. Lee, W.-C. Wu, C.-C. Wang, Encapsulating curcumin in ethylene diamine-β-cyclodextrin nanoparticle improves topical cornea delivery, Colloids Surf. B Biointerfaces 186 (2020) 110726, https://doi.org/10.1016/j.colsurfb.2019.110726.
[47] P. Sadeh, S. Zeinali, B. Rastegari, I. Najafipour, Size optimization of mesoporous β-Cyclodextrin Metal-Organic frameworks as Bio-MOFs, J. Cryst. Growth 620 (2023) 127348, https://doi.org/10.1016/j.jcrysgro.2023.127348.
[48] B. Lin, H. Chen, D. Liang, W. Lin, X. Qi, H. Liu, X. Deng, Acidic pH and high-H2O2 dual tumor microenvironment-responsive nanocatalytic graphene oxide for cancer selective therapy and recognition, ACS Appl. Mater. Interfaces 11 (2019) 11157–11166, https://doi.org/10.1021/acsami.8b22487.